# Fast Water Channeling across Carbon Nanotubes in Far Infrared Terahertz Electric Fields

Qi-Lin Zhang[1,2], Rong-Yao Yang[1], Wei-Zhou Jiang[1,*], Zi-Qian Huang[1]

[1] *Department of Physics, Southeast University, Nanjing 211189, China*

[2] *Department of Mathematics and Physics, Anhui Polytechnic University, Anhui 241000, China*

Using molecular dynamics simulations, we investigate systematically the water permeation properties across the single-walled carbon nanotube (SWCNT) in the presence of the terahertz electric field (TEF). With the TEF normal to the nanotube, the fracture of the hydrogen bonds results in the giant peak of net fluxes across the SWCNT with a three-fold enhancement centered around 14THz. The phenomenon is attributed to the resonant mechanisms, characterized by librational, rotational, and rotation-induced responses of in-tube polar water molecules to the TEF. For the TEF along the symmetry axis of the nanotube, the vortical modes for resonances and consequently the enhancement of net fluxes are greatly suppressed by the alignment of polar water along the symmetry axis, which characterizes the quasi one-dimensional feature of the SWCNT nicely. The resonances of water molecules in the TEF can have potential applications in the high-flux device designs used for various purposes.

## I. INTRODUCTION

The study of the water molecular transport in nanochannels is important not only for the basic research and potential applications but also for the understanding of the water permeation in biological channels. Indeed, one important reason why research on nanochannel transport properties has continued to be of interest is that many primary characteristics of water confined in simple nanochannels are similar to that of complex biological channels[1–7]. In the past, the water transport properties have been studied extensively in single-walled carbon nanotubes (SWCNTs)[8–12]. Novel studies on water transports in nanochannels have continued to appear in recent years with various designs concerning temperature gradients[13], charge modification[14], coulomb dragging[15], collective mode oscillations[16], and phonon-induced frictions[17]. Besides the biological implications in these studies, the stream of these novel progresses may potentially become integrated into the application pool for the design of innovative nanofluidic devices, such as flow sensors[18], desalination of seawater[19], molecular sieves[20], and so on.

Recently, broad interest has been aroused to study the electric field (EF) effects on the water permeation [21–31]. It is known that the applied EF can stem from electromagnetic radiations. A well-known example is the laser-generated EF that has fascinating applications, e.g., see[32,33]. Nowadays, high-power terahertz (THz) radiation can be generated progressively, say, by optical rectification methods[34], linear accelerators[35,36], and laser-driven ion or electron accelerators[37,38]. The consequent THz EF (TEF) of the order of GV/m, generated by focusing high-power THz rays, can open up a new era to study structural transitions in polar molecules given the TEF-driven molecular rotations over random thermal motions. Such studies are of fundamental impor-

tance in revealing the mechanism for molecular motors that produce directional motion[39–42]. While for water permeation in nanochannels, the study of TEF effects is scarcely found in the literature, and no attention has been paid to the role of the TEF-driven molecular rotations. It is thus of prime significance for us to first reveal whether and how the TEF-driven molecular rotations and intrinsic mechanisms affect the water flow. A clear understanding of the TEF effects is also very instructive to develop new devices for efficient water filtration and energy transfer. Using molecular dynamics (MD) simulations, we have observed that water permeation properties can greatly be affected by the TEF through rotational and rotational-induced translational resonances in a broad THz frequency range.

## II. COMPUTATIONAL METHODS

The MD simulation system built with the molecular visualization program[43] is illustrated in Fig. 1. An uncapped (6,6) armchair SWCNT with a length of 1.34 $nm$ and a diameter of 0.81 $nm$ is embedded in two parallel graphite sheets along the $z$ direction. The distance between the bottom end of the SWCNT and the graphite sheet is 2 $\overset{\circ}{A}$. MD simulations are performed using the NAMD2[44] in a $NVT$ ensemble with the initial box sizes of $L_x = 3.5$ $nm$, $L_y = 3.5$ $nm$, $L_z = 6.3$ $nm$, constant temperature (300 $K$) achieved by the Langevin dynamics with a damping coefficient of 1 $ps^{-1}$, and periodic boundary conditions in all directions. The electrostatic interactions are handled by the particle mesh Ewald method[45] with a real space cutoff of 1.2 $nm$, and the cutoff for the van der Waals interaction is also 1.2 $nm$. The CHARMM27 force field[46,47], TIP3P water model[48] and SHAKE algorithm for bond lengths[49] are adopted in all the simulations. The time step is 1 $fs$. To obtain a directed flow[47], an acceleration of 0.01 $nm$ $ps^{-2}$ per water molecule is imposed along $+z$ direction to produce a pressure difference between two ends of the SWCNT

about 20 $MPa$[10]. The carbon atoms at the inlet and outlet are fixed and other atoms of the SWCNT are flexible to prevent possible errors from the rigid wall[10,50].
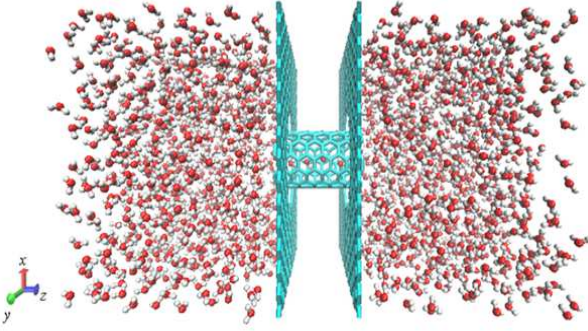


FIG. 1: (Color online) Snapshot of the simulation system. An uncapped (6,6) armchair SWCNT combined with two graphite sheets is solvated in a water box of $3.5 \times 3.5 \times 6.3 nm^3$ with 1852 molecules. There is a vacuum between the two sheets. The axis of SWCNT is parallel to the z-axis. To obtain the net flux, an acceleration of each water molecule is imposed, see text.

In our simulations, only the space between two reservoirs is exposed to the spatially uniform TEF, and a justification for this setup is given in the Supporting Material[51]. With the EF direction being parallel to the x-axis, the TEF, acted on the atomic partial charges, can be expressed as

$$\mathbf{E} = E_0(\cos(\omega t), 0, 0). \tag{1}$$

In this work, we take the amplitude of the EF $E_0 = 1 V/nm$[27,52] along the x-axis, unless otherwise denoted, and consider the frequencies ranging from 0.1 to 40 $THz$. Hereafter, these far infrared EFs are still dubbed the TEF, since the interesting results lie below the region over a dozen THz. It is known that the electric and magnetic fields of the electromagnetic wave obey the relation $|\mathbf{E}/\mathbf{B}| = c$ where $c$ is the speed of light. Because the speed of water molecules inside nanotubes is far less than the speed of light, the Lorentz force is negligibly small in comparison to the electric force. Thus, we neglect the effect of the magnetic field in our estimation.

We should point out that the fast water transport desired in this work is different from the in-tube water pumping by the AC electric field[21,22]. For water pumping through SWCNTs, the energy acquisition in the AC field is necessary, and simultaneously the spatial asymmetry should be temporally retained in a delicate thermodynamic relaxation process. Our simulations with the symmetric setup in the uniform TEF are carefully testified to have null pumping under zero pressure gradient.

## III. RESULTS AND DISCUSSIONS

Simulations are performed for the system within the EF at different frequencies. For each frequency, the simulation time is 45 ns, and the last 40 ns is collected for analysis. For clarity, here the net flux is defined to be the difference between the water molecular number per nanosecond across the SWCNT from one end to the other[6,10]. The average occupancy [1,10] and hydrogen bond numbers of water molecules inside the SWCNT are denoted by the symbol $\bar{N}$ and $\bar{N}_H$, respectively.

The net water fluxes, as a function of the EF frequency, are shown in Fig. 2 where the zero-field ($E_0 = 0$) net flux (about 21 $ns^{-1}$) is also displayed. We see that with the EF along the x-axis the net fluxes can be characterized by a giant peak centered at 14 $THz$ with a three-fold enhancement of the flux. In sharp comparison to the zero-field result, the dramatic enhancement of the water flux is observed in the frequency range around 10 $THz$ to 20 $THz$. For much lower or higher frequencies, the net flux falls off, being close to the one of the zero field. For the net fluxes with the EF along the z-axis, also displayed in Fig. 2, the enhancement is greatly suppressed. This distinct phenomenon, associated with the z-direction polarization of in-tube water molecules, characterizes interestingly the property of the quasi one-dimensional SWCNT.
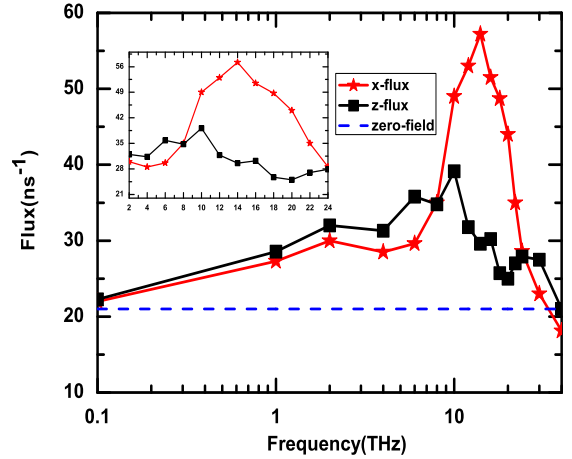


FIG. 2: (Color online) The net flux as a function of the EF frequency. The curves with stars and squares stand for results with the EF along x- and z-axes, respectively. The dash line denotes the zero-field flux. The window amplification within 2-24 $THz$ is exhibited in the inset.

The extraordinary characteristics of the water transport should uniquely be determined by the behaviors of the in-tube water in the applied TEF. We thus count the number of hydrogen bonds $\bar{N}_H$ inside the SWCNT in the frequency range as shown in Fig. 3, according to the criterion of the oxygen distance less than 3.5 $\overset{\circ}{A}$ and hydrogen-bond angle $\leq 30°$[6]. It is observed that the $\bar{N}_H$ values are about 3.01, 2.97, 0.81, 0.61, 1.26 and 2.97 at
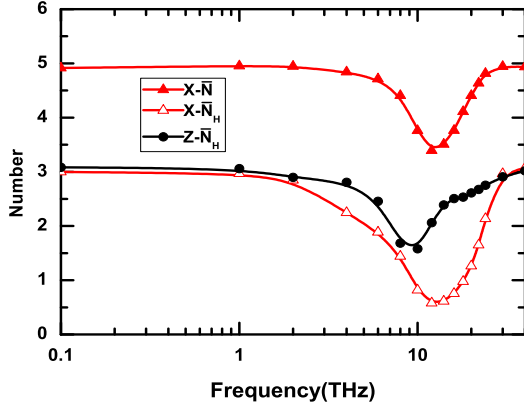
FIG. 3: (Color online) The average occupancy number $\bar{N}$ and hydrogen bond number $\bar{N}_H$ of water molecules inside the SWCNT as a function of the EF frequency in the $x$- or $z$-direction field, as denoted.
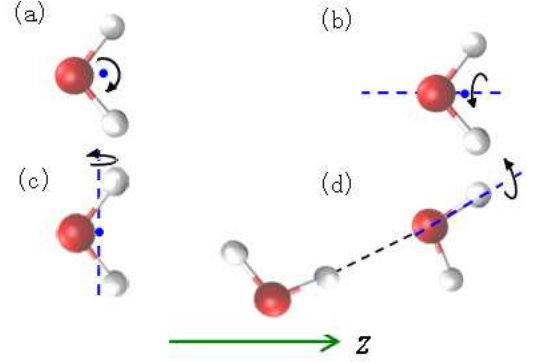


FIG. 4: (Color online) The water molecule revolves along (a), the axis vertical to the water molecule plane through the center of mass, (b), the symmetry axis, (c), the axis through the center of mass but parallel to the connecting line of two hydrogen atoms, and (d), the axis on the hydrogen bond, respectively.

0.1, 1, 10, 14, 20 and 30 $THz$, respectively. The minimum of the $\bar{N}$ is about 3.5 at 14 $THz$. As shown in Figs. 2 and 3, the deep valley around 14 $THz$ in the frequency profile of the $\bar{N}_H$ corresponds to the giant peak of the flux and the moderate dip of the number of water molecules in the SWCNT, exhibiting a characteristic resonant phenomenon. In the whole frequency region interested in this work, we see that the variation of the flux takes place coherently with those of the numbers of hydrogen bonds and water molecules inside the SWCNT. The dramatic drop of the hydrogen-bond number is a result of the breaking of hydrogen bonds, while the latter drives the sudden rise of the net flux.

Under the equilibrium condition, the in-tube water transports in correlated bursts of the hydrogen-bonded filament[1,2], the net flux increases linearly with the pressure gradient. The water transports at equilibrium can also be demonstrated by the collective diffusion model[9]. Here, the dramatic rise of the net flux occurs with the rupture of hydrogen bonds due to the energy transfer from the TEF (see Supporting Material[51]). The large kinetic energy of water molecules acquired then leads to fast shuttling of the water molecules from one end to the other and correspondingly the dramatic rise of the flux. In this case, the energy transfer from the TEF spoils the spontaneous diffusion due to the thermal fluctuation at equilibrium, and we cannot follow simply the collective diffusion model under the non-equilibrium condition. In the frequency range without significant breaking of hydrogen bonds, the fluxes in the presence of the pressure gradient are consistent with those given by the approach by Zhu et al[9]. In the case of dramatic rupture of hydrogen bonds, the relation between the net flux and the pressure gradient is not far off linear in a large domain of the pressure gradient, see Ref.[51], though in this case the equilibrium diffusion does not apply at null pressure.

Now, we need to reveal the underlying mechanism for the fracture of hydrogen bonds. Undoubtedly, the EF can't generate directly the translational motion of charge neutral molecules, but can drive the vortical motion of polar water molecules to acquire the energy. Shown in Fig. 4 are four representative vortical modes with different rotational axes. The vortical motion can be transmitted to the wobbling of the molecular center of mass in the vertical section due to the hydrogen-bond locking together with the thermodynamical motion. As a result, this provides a pathway to vibrational resonances to shake off the hydrogen bonding, while the resonant frequency range is estimated around 4-14 $THz$, according to the equality of the energies of the water molecule binding and the harmonic oscillator[16]. Besides the vibrational resonances, the TEF can generate direct rotational resonances. Due to the hydrogen bonding of water molecules, all the vortical motions should be, in principle, the reciprocating motions rather than the strict rotation. For convenience, we make somehow discretionary identifications for vortical modes in Fig. 4: 4(a), (b), and (c) are three independent rotational modes whose rotational axes are the principal axes, and 4(d) the librational mode for the hydrogen bonding. Now, we use the rotor model to estimate the resonant frequency for rotational or librational motions: $E_b = I\omega^2/2$ where $E_b$ is the binding energy of each water molecule, and $I$ is the moment of inertia of the water molecule. If $I$ is the total moment of inertia, the energy of a rotor can be re-expressed by the components on the three principal axes. Using the value of $E_b = 16$ $kcal/mol$[1], the resonant frequencies of the water molecule are estimated to be about 14, 17, 24 and 20 $THz$, corresponding to the modes in Fig. 4(a), (b), (c), and (d), respectively. Besides four specific cases, the axes can tilt for the thermal motion. Consequently, the change of the moment of inertia results in the continuation to neighboring frequency domains of the characteristic modes above.

To evidence these resonant mechanisms, we first do a test by extending the TEF to the reservoirs at both sides. We find nearly a five-fold enhancement of the net flux in

the frequency range of 4-24 *THz*, while beyond this frequency range the flux drops off rapidly. The reason for this to occur is that the water molecules liberated from the hydrogen bonding in the reservoir can break into the nanotube rather freely. In addition, the flux enhancement is almost independent of the TEF orientation in this case. As the TEF over the reservoirs withdraws, some distinct behaviors are exhibited for the single-filed water chain in the SWCNT. We see from Fig. 3 that the breaking of hydrogen bonds is not efficient below $8\,THz$ because of the SWCNT suppression of the needed large-amplitude vibration. We also see that the breaking of hydrogen bonds through the rotational mode of Fig. 4(c) is of low efficiency in that the coherent flip does take the priority for the constraint of the SWCNT. In these cases, the suppression of the flux occurs correspondingly, as shown in Fig. 2. In the $x$-direction TEF, an apparent resonant phenomenon, characteristic of a giant peak, thus arises eventually. We can see that the resonant frequencies given by the rotor model are consistent with the large fluxes and small hydrogen bond numbers shown in Figs. 2 and 3. For the $z$-direction TEF, we see that the rotational mode of Fig. 4 (b) is out of operation. Indeed, all the vortical modes in the $z$-direction TEF are largely suppressed by the forced alignment along the $z$-axis. As a result, the giant peak crashes down, as shown in Fig. 2.

In the low-frequency range roughly below 1 *THz*, the difference from the zero-field flux can be attributed to the alignment of the polar molecules along the EF. The change of the alignment direction in the low-frequency TEF yields coherently the flips of the water chain, resulting in the moderate enhancement of the flux. With the $z$-direction TEF, the polar water may be aligned along the $z$-axis, the wobbling and random motions in the transverse section are largely suppressed with the enhancement of the ordered permeation. This interprets that the net fluxes remain a little larger than those of the $x$-direction TEF at low frequencies. At higher frequencies ($f > 30\ THz$), being far away from the resonant range, the phenomenon evolves trivially, being close to the zero-field results.

To comprehend the transport behaviors in the TEF in more details, we now examine the average dipole orientations of the water chain. Fig. 5 shows the probability distributions of the average angle $\langle\theta\rangle$ of water molecules inside the SWCNT for different frequencies, where $\theta$ represents the angle between the symmetry axis of the water molecule [see Fig. 4(b)] and the $z$-axis. The average is performed over all the water molecules inside the SWCNT in last 40 *ns* of the simulation time. As shown in Fig. 5, only for the zero-field case exists the single peak with the peak value around 30°, in accord with previous studies[28,53]. Note that the symmetric orientation distribution around 30° and 150° at the zero field can be anticipated under small pressure gradients, because in this case low speeds of water molecules can yield sufficient time to produce significant flips in the nanotube. With the frequency at 0.1, 1, 24 and 40 *THz* appears remarkably the double-peak structure, serving
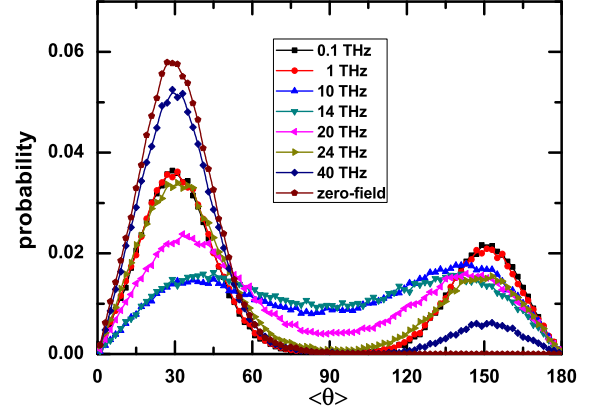


FIG. 5: (Color online). Probability distributions of the dipole orientation of water molecules inside the tube for different EF frequencies.

as the signature of the frequent flip of water molecules. The flip may occur for some perturbation of the form like $e^{i\omega t}$ in a sufficient time span. The noticeable fact is that the double-peak structure becomes flattened for the frequencies within the top region of the resonant peak in Fig. 2, say, 10 , 14 and 20 *THz*, as shown in Fig. 5. This provides a specific evidence for the hydrogen bond fracture in the resonant zone. It is the release of water from the hydrogen bonding that smears out the specific orientations peaked around 30° and 150°. Note that the less flattening for the 20 *THz* curve is also consistent with the farther distance from the peak value as shown in Figs. 2 and 3.

In addition, the resonance can be well visualized in a dynamic evolution of hydrogen bonds for water molecules confined in the SWCNT. We observe that the average numbers of hydrogen bonds at 0.1 and 30 *THz* remain almost unchanged from 0 to 10 *ps*. However, we observe that in the frequency range of 10-20 *THz* the hydrogen-bond number starts to reduce explicitly within 1 ps. These exemplifications indicate that resonant response of the water chain to the TEF is rather prompt once the strong torque is exerted on the water molecule.

It is worthwhile discussing the dependence of the water transport on the TEF amplitude. We find that the average hydrogen bond number and the net flux do not undergo significant differences for $E_0 = 1$ and a few V/nm. However, for the $E_0$ below 1 *V/nm*, the TEF effect on the water transport fades away quickly with the decrease of the TEF amplitude. For instance, at $E_0 = 0.1\ V/nm$, the average hydrogen bond number and the net flux are similar to their zero-field results, respectively. The reason of this phenomenon lies in the fact that the small-amplitude TEF can not produce sufficient torque to win the competition with the thermal fluctuations of the water molecules. It is also significant to explore the resonant effects on the water transport in much longer SWCNTs

that is easier to connect with the experiments. In the SWCNT with the length of 10 *nm*, we have observed the similar rupture of hydrogen bonds. The flux enhancement due to the rupture of hydrogen bonds is also about 3-fold at the same pressure gradient as that for the short SWCNT. Moreover, we have studied the water transport properties at much smaller pressure gradients. It is observed that the resonant phenomenon is not changed by the magnitude of pressure gradient. We perform, as an example, the simulation with the frequencies 10 and 14 *THz*. Compared to net fluxes at non-resonant frequencies, the significant flux enhancement remains at lower pressures. For details, see the Supporting Material[51].

We notice that the TEF should be regarded as the effective field of the THz radiation penetrating the tube because of the partial screening by the electron clouds laying on the SWCNT. It is of interest to consider later on whether the radial breathing mode (RBM) of the SWCNT can be efficiently generated by the TEF and how RBM-induced vibrations mix with the direct TEF-driven modes[16]. In addition, we would mention that simulations with polarizable models for conducting carbon nanotubes do not produce appreciable difference in the water transport, compared with those with nonpolarizable models for semiconducting carbon nanotubes[54,55]. Finally, in order to examine the model dependence, we performed some comparative simulations using the SPC/E water model[56,57]. Though the magnitude of the flux with the TIP3P water model is different from the one obtained with the SPC/E model, the tendencies of the net flux, the hydrogen-bond and occupancy numbers with both models are consistent with each other. Thus, the main conclusions that we have drawn do not depend on the specific water model. For details, see Ref.[51].

## IV. CONCLUSIONS

In summary, we have demonstrated the effects of the vortical resonant mechanisms in the TEF on the transport properties and dynamical behaviors of water molecules across the SWCNT. The resonances, resulting from librational, rotational and rotation-induced translational modes of polar water molecules, generate significant hydrogen-bond fractures and consequently the dramatic enhancement of the net flux, with the TEF normal to the SWCNT. The resonant phenomenon is well established. The change shows up when the TEF turns to the symmetry axis of the nanotube: the resonant phenomenon is greatly suppressed by the alignment of water molecules along the symmetry axis, which characterizes the quasi one-dimensional feature of the SWCNT. Our work suggests that the TEF resonant mechanisms are instructive to develop high-flux nanoscale devices and explore possible implications for the biological water channelling.

1 G. Hummer, J. C. Rasaiah, and J. P. Noworyta, Nature **2001**, 414, 188-190.

2 A. Waghe, J. C. Rasaiah, and G. Hummer, J. Chem. Phys. **2002**, 117, 10789.

3 B. L. de Groot and H. Grubmuller, Science **2001**, 294, 2353-2357.

4 A. Anishkin and S. Sukharev, Biophys. J. **2004**, 86, 2883-2895.

5 O. Beckstein and M. S. P. Sansom, Proc. Natl. Acad. Sci. U.S.A. **2003**, 100, 7063-7068.

6 R. Z. Wan, J. Y. Li, H. J. Lu, and H. P. Fang, J. Am. Chem. Soc. **2005**, 127, 7166-7170.

7 O. Beckstein, *et al.*, J. Phys.Chem. B **2001**, 105, 12902-12905; A. V. Raghunathan and N. R. Aluru, Phys. Rev. Lett. **2006**, 97 024501; P. Gallo, *et al.*, J. Chem. Phys. **2000**, 113, 11324-11335; L. Kullman, *et al.*, Biophys. J. **2002**, 82, 803-812.

8 K. Murata, K. Mitsuoka, T. Hirai, T. Walz, P. Agre, J. B. Hemann, A. Engel, and Y. Fujiyoshi, Nature **2000**, 407, 599-605.

9 F. Q. Zhu, E. Tajkhorshid, and K. Schulten, Phys. Rev. Lett. **2004**, 93, 224501.

10 X. J. Gong, J. Y. Li, H. J. Lu, H. Zhang, R. Z. Wan, and H. P. Fang, Phys. Rev. Lett. **2008**, 101, 257801; X. J. Gong, J. C. Li, K. Xu, J. F. Wang, and H. Yang, J. Am. Chem. Soc. **2010**, 132, 1873-1877.

11 J. K. Holt *et al.*, Science **2006**, 312, 1034-1037.

12 S. Joseph and N. R. Aluru, Nano Lett. **2008**, 8, 452-458.

13 M. J. Longhurst and N. Quirke, Nano Lett. **2007**, 7, 3324-3328.

14 J. Y. Li, X. J. Gong, H. J. Lu, D. Li, H. P. Fang, and R. H. Zhou, Proc. Natl. Acad. Sci. U.S.A. **2007**, 104, 3687-3692.

15 B. Wang and P. Kra, J. Am. Chem. Soc. **2006**, 128 15984-15985.

16 Q. L. Zhang, W. Z. Jiang, J. Liu, R. D. Miao, and N. Sheng, Phys. Rev. Lett. **2013**, 110, 254501.

17 M. Ma, F. Grey, L. Shen, et al. Nat. Nanotech. **2015**, 10, 692-695.

18 S. Ghosh, A. K. Sood and N. Kumar, Science **2003**, 299, 1042-1044.

19 B. Corry, J. Phys. Chem. B **2008**, 112, 1427-1434.

20 K. B. Jirage, J. C. Hulteen, and C. R. Martin, Science **1997**, 278, 655-658.

21 D. J. Bonthuis, D. Horinek, L. Bocquet,and R. R. Netz, Langmuir **2010**, 26, 12614-12625.

22 K. F. Rinne, S. Gekle,D. J. Bonthuis,and R. R. Netz, Nanoletters **2012**, 12, 1780-1783.

23 M. White and N. Quirke, Nat. Nanotech. **2007**, 2, 87-94.

[24] X. Xin, H. Altan, A. Saint, D. Matten, and R. R. Alfano, J. Appl. Phys. **2006**, 100, 094905.

[25] Y. C. Choi, C. Pak, and K. S. Kima, J. Chem. Phys. **2006**, 124, 094308.

[26] J. A. Garate, N. J. English, and J. M. D MacElroy, J. Chem. Phys. **2009**, 131, 114508.

[27] X. P. Li, G. P. Kong, X. Zhang, and G. W. He, Appl. Phys. Lett. **2013**, 103, 143117.

[28] J. Y. Su and H. X. Guo, ACS Nano. **2011**, 5, 351-359.

[29] L. Figueras and J. Faraudo, Molecular Simulation **2012**, 38, 23-25.

[30] J. L. Kou, H. J. Lu, F. M.Wu, *et al.*, Nano Lett. **2014**, 14, 4931-4936

[31] J. Kou, J. Yao,H. LU, *et al.*, Angew. Chem. Int. Ed. **2015**, 54, 2351-2355.

[32] Y. I. Salamin, S. X. Hu, K. Z. Hatsagortsyan, C. H. Keitel, Phys. Rep. **2006**, 427, 41-155.

[33] Th. Fennel, K. H. Meiwes-Broer, J. Tiggesbäumker, *et al.*, Rev. Mod. Phys. **2010**, 82, 1793.

[34] A. G. Stepanov, L. Bonacina, S. V. Chekalin, and J.-P. Wolf, Opt. Lett. **2008**, 33, 2497-2499.

[35] G. L. Carr, M.C. Martin, W. R. McKinney, K. Jordan, G. R. Neil, and G. P. Williams, Nature **2002**, 420, 153-156.

[36] S. Casalbuoni, B. Schmidt, P. Schmüser, V. Arsov, and S. Wesch, Phys. Rev. ST Accel. Beams **2009**, 12, 030705.

[37] A. Gopal, S. Herzer, A. Schmidt, *et al.*, Phys. Rev. Lett. **2013**, 111, 074802.

[38] A. Pukhov, I. Kostyukov, T. Tückmantel, Ph. Luu-Thanh, G. Mourou, Eur. Phys. J-Spec. Top. **2014**, 233, 1197-1206.

[39] S. P. Fletcher, F. Dumur, M. M. Pollard, and B. L. A. Feringa, Science **2005**, 310, 80-82.

[40] J. S. Seldenthuis, F. Prins, J. M. Thijssen, and H. S. J. van der Zant, ACS Nano. **2010**, 4, 6681-6686.

[41] H. L. Tierney, C. J. Murphy, A. D. Jewell, *et al.* Nat. Nanotech. **2011**, 6, 625-629.

[42] Q. C. Zhang, F. T. Wu, H. M. Hao, H. Xu, H. X. Zhao, *et al.*, Angew. Chem. **2013**, 125, 12834-12837.

[43] W. Humphrey, A. Dalke, and K. Schulten, J. Molec. Graphics **1996**, 14, 33-38.

[44] J. C. Phillips *et al.*, J. Comput. Chem. **2005**, 26, 1781-1802.

[45] T. A. Darden, D. M. York, and L. G. Pedersen, J. Chem. Phys. **1993**, 98. 10089-10092.

[46] A. D. MacKerell *et al.*, J. Phys. Chem. B **1998**, 102, 3586-3616.

[47] F. Q. Zhu, E. Tajkhorshid, and K. Schulten, Biophys. J. **2002**, 83, 154-160.

[48] W. L. Jorgensen, J. Chandrasekhar, J. D. Madura, R. W. Impey, and M. L. Klein, J. Chem. Phys. **1983**, 79, 926-935.

[49] J. P. Ryckaert, G. Ciccotti, and H. J. C. Berendsen, J. Comput. Phys.**1977** 23, 327-341.

[50] A. Martini, H. Y. Hsu, N. A. Patankar, and S. Lichter, Phys. Rev. Lett. **2008** 100, 206001.

[51] Q. L. Zhang, R. Y. Yang, W. Z. Jiang, and Z. Q. Huang, Supporting Material, submitted in 2015.

[52] S. D. Luca, B. D. Todd, J. S. Hansen, and P. J. Daivis J. Chem. Phys. **2013**, 138, 154712.

[53] G. Zuo, R. Shen, S. Ma, W. Guo, ACS Nano **2009**, 4, 205.

[54] S. Joseph and N. R. Aluru, Phys. Rev. Lett. **2008**, 101, 064502.

[55] F. Moulin, M. Devel, and S. Picaud, Phys. Rev. B **2005**, 71, 165401.

[56] H. Berendsen, J. Grigera, and T. J. Straatsma, Phys. Chem. **1987**, 91, 6269-6271.

[57] P. Mark and L. Nilsson, J. Phys. Chem. A **2001**, 105, 9954-9960.